Modular Multilevel DC Converter : Impact of the Control on the Design and Efficiency

Johan Boukhenfouf, Pierre Vermeersch, Francois Gruson, Philippe Delarue, Philippe Lemoigne, Frédéric Colas, Xavier Guillaud

Modular Multilevel DC Converter : Impact of the Control on the Design and Efficiency

Johan BOUKHENFOUF, Pierre VERMEERSCH, Francois GRUSON, Philippe DELARUE, Philippe LEMOIGNE, Frédéric COLAS, Xavier GUILLAUD
Univ. Lille, Arts et Métiers Institute of Technology, Centrale Lille, Junia, ULR 2697 - L2EP
F-59000 Lille, France
E-Mail: johan.boukhenfouf@ensam.eu, francois.gruson@ensam.eu
URL: https://l2ep.univ-lille.fr/en/

***Index Terms*—DC-DC converter, Modular Multilevel Converters (MMC), HVDC**

***Abstract*—The Modular Multilevel DC Converter is an attractive non-isolated topology to inter- connect High Voltage DC Links. This paper presents the interaction among control, component design and efficiency of this converter. The impact of the two degrees of freedom on the design and the efficiency is analyzed.**

NOMENCLATURE

The upper and lower arms are precised with the subscript "u" and "l".

P^*	Reference power on low-voltage side
C_{SMu},C_{SMl}	Capacity of submodules
C_{totu},C_{totl}	Equivalent capacity of arm
i_s	Current on low-voltage side
i_{diff}	Differential current
v_{diff},v_s	Decoupled modulated voltages.
v_{Ctotu},v_{Ctotl}	Voltage of equivalent capacity of arm
N_u, N_l	Number of submodules in the arm
n_u, n_l	Number of active submodules in the arm
v_{mu};v_{ml}	Modulated voltages
ω	Pulsation of AC variables
θ	Angle between i_{sAC} and i_{diffAC}
φ	Angle between the AC components of v_{ml} and $-v_{mu}$
θ_v	Anle between v_{sAC} and v_{diffAC}
R_{arm}	Arm resistance
L_{arm}	Arm inductance
R_s, R_s	Line resistance and inductance
$W_c^{\sum}$	Energy stored in the leg
W_c^{Δ}	Difference of energy stored between the upper leg and the lower leg.

I. INTRODUCTION

Over the last decades, numerous HVDC links have been put into service and many others are planned. To increase their reliability and flexibility, DC multi-terminal high voltage networks (MTDC) were proposed. As the projects of HVDC links were not coordinated, there are different technologies (LCC, VSC), configurations and grounding scheme. Hence, bidirectional DC-DC converters will be needed for the interconnection. Due to the high voltages, conventional DC-DC converters cannot be employed. For this range of voltages, the main converters are based on the modular multilevel converter [1], [2]. Within this group, the modular multilevel DC converter (M2DC), showed in fig. 1, is a non-isolated topology with a high potential. It is composed of at least two legs of submodules interconnected between the two DC grid [3]. submodules may be half-bridge or full-bridge depending on the need of DC fault blocking capability. As an asymmetrical monopolar converter, the M2DC can be extended to bipolar operation by using two converters : one with a positive voltage, the other with negative one.

Over the past 15 years, the original AC-DC MMC converter has been the source of significant research. Lately, it also has inspired various topologies for DC-DC converters, for instance the MMC dual active bridge, the auto dc-transformer or the M2DC. There are not many studies on the latter. Some control challenges were identified in [4]. [5], [6] offer partial studies on the design and control of the M2DC. [7] proposes an explicit control of all state variables of the converter to minimize the circulating currents by using the degrees of freedom of the control : the frequency and the angle. However, lower currents does not necessarily mean less losses [8] due to the nonlinear nature of converters. So, this paper means to analyze the impact of these degree of freedom

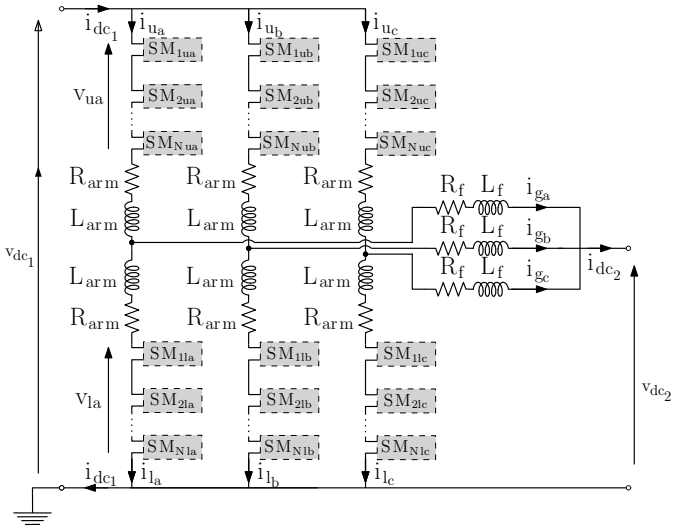

Fig. 1: Diagram of M2DC converter with three legs.

on the design of components and on the efficiency of the converter.

First, the general principal of the M2DC are reminded. Secondly, a quasi-static analysis of one leg is carried out. Thirdly, the interaction between the control choices and the design is presented.

II. Principle of operation of M2DC and average model

This first part presents the operating principle of the M2DC converter. The converter considered has three legs as a classical AC-DC MMC. The analysis is the same for each leg, so, it is only realized on one leg.

To begin, the DC power transfer is examined. Consider v_{muDC}, v_{mlDC}, the DC components of the modulated voltages and i_{uDC}, i_{lDC} the DC components of the leg currents. If the losses in the resistances and the conduction losses in the submodules are neglected, v_{muDC}, v_{mlDC}, i_{uDC}, i_{lDC} can be expressed as in (1).

$$\begin{aligned} v_{muDC} &= v_{dc_1} - v_{dc_2} & i_{uDC} &= i_{dc_1} \\ v_{mlDC} &= v_{dc_2} & i_{lDC} &= i_{uDC} - i_{sDC} \end{aligned} \tag{1}$$

Consider P, the power flowing through the legs from the high-voltage side to the low-voltage side, then the DC power of the upper and lower arms is given in (2).

$$\begin{aligned} P_{uDC} &= v_{muDC} i_{uDC} &&= (1-\alpha)P \\ P_{lDC} &= v_{mlDC} i_{uDC} &&= (\alpha-1)P \end{aligned} \text{ with } \alpha = \frac{v_{dc2}}{v_{dc1}} \tag{2}$$

As showed by the above equation, the DC power flowing in the leg is opposite in each arm but more importantly it is non-zero. So, the energy stored in the capacitors will diverge. To avoid this, AC components are introduced in the converter in order to nullify the average power of the arms. So v_{mu} and v_{ml} can be expressed as in (3).

$$\begin{aligned} v_{mu}(t) &= v_{muDC} + \sqrt{2} V_{muAC} cos(\omega t + \theta_{vmu}) \\ v_{ml}(t) &= v_{mlDC} + \sqrt{2} V_{mlAC} cos(\omega t + \theta_{vml}) \end{aligned} \tag{3}$$

The objective of the control is to generate the alternative component of the modulated voltages to stabilizes the energy stored in the capacitor. As the three legs are identical, the study will be carried out only for one. Moreover, due to the numerous submodules in the converter, the analysis is simplified using the average leg model of fig. 2 [9]. The hypothesis for this approximation is the proper operation of the capacitor voltage balancing algorithm. This model is independent of the type of submodules (half-bridge or full-bridge).

In the average leg model, the submodule stack is represented by one equivalent capacitor alimented by a perfect chopper. The capacitor voltage v_{Ctot} is the sum of the submodules capacitor voltages. Its behaviour is expressed in (4). The current going through this capacitor is the modulated current i_{Ctot} that comes from the perfect chopper. The duty cycle is equal to the number of activated submodules divided by the total number of submodules. The modulated voltage of the arm v_m is the chopped voltage from v_{Ctot}. (5) summarized the relations of the perfect chopper. The subscript *j* indicates the upper or lower leg.

$$C_{tot} \frac{dv_{Ctotj}}{dt} = i_{Ctotj} \quad \text{with } C_{tot} = \frac{C_{SMj}}{N_j} \tag{4}$$

$$\begin{aligned} v_{mj} &= m_j v_{Ctotj} \\ i_{Ctotj} &= m_j i_j \end{aligned} \text{ with } mj = \frac{n_j}{N_j} \tag{5}$$

In this paper, in order to present the control and the operating principal clearly, the capacitors values C_{totu} and C_{totl} are firstly supposed equal.

The average leg model of the M2DC contains four independent state variables. The upper and lower equivalent capacitor voltages (v_{ctotu}, v_{ctotl}) and two currents (it can be the arm currents or one arm current and the output current for example). Therefore, four controllers are needed : one for each independent state variable. Furthermore, it is reminded that the DC component controls the power flow through the converter. That is to say, it manages the input/output power. Meanwhile, the AC component handles the stability of the stored energy in the converter.

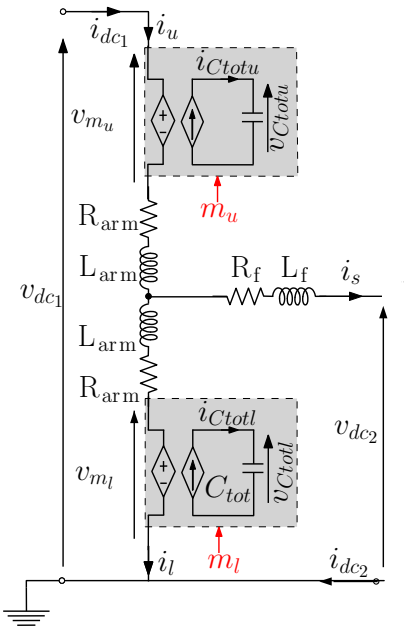

Fig. 2: Equivalent average arm model.

III. Quasi-static analysis of one leg

A. Instantaneous voltage and currents

In the first place, Kirchhoff describes the relations among currents and voltages in the converter. As in the MMC converter, this equations are coupled between state variables. To uncouple the system, a change of variable is necessary. The new variables for the control are defined in (6).

$$\begin{cases} v_{diff} = \dfrac{v_{mu} + v_{ml}}{2} \\ i_{diff} = \dfrac{i_u + i_l}{2} \end{cases} \qquad \begin{cases} v_s = \dfrac{v_{mu} - v_{ml}}{2} \\ i_s = i_u - i_l \end{cases} \tag{6}$$

With that new set of variables, the system can be described with equations (7) and (8) for the DC components.

$$\frac{v_{dc1}}{2} = L_{arm}\frac{di_{diff}}{dt} + R_{arm}i_{diff} + v_{diff} \tag{7}$$

$$\frac{v_{dc1}}{2} - v_{dc2} = L_s\frac{di_s}{dt} + R_s i_s + v_s \tag{8}$$

$$\text{with } L_s = \frac{L_{arm}}{2} + L_f \tag{9}$$

Similarly, the equations for the AC components are (10) and (11).

$$0 = L_{arm}\frac{di_{diff}}{dt} + R_{arm}i_{diff} + v_{diff} \tag{10}$$

$$0 = L_s\frac{di_s}{dt} + L_s i_s + v_s \tag{11}$$

The current model of the M2DC is established. The control loops are determined with the model inversion principal as presented in [7]. The resulting currents and voltages will be composed of a DC component and an AC compopent as showed by (12)-(15).

$$i_{diff}(t) = i_{diffDC} + \sqrt{2}I_{diffAC}cos(\omega t) \tag{12}$$

$$i_s(t) = i_{sDC} + \sqrt{2}I_{sAC}cos(\omega t - \theta) \tag{13}$$

$$v_{diff}(t) = v_{diffDC} + \sqrt{2}V_{diffAC}cos(\omega t + \theta_{diff}) \tag{14}$$

$$v_s(t) = v_{sDC} + \sqrt{2}V_{sAC}cos(\omega t - \theta_v + \theta_{diff}) \tag{15}$$

Each component must be defined to obtain the full model of the converter. Using the superposition theorem, the DC and AC components are controlled independently.

B. Model of the DC components

Firstly, the DC components are studied. Consider P the power injected on the low-voltage side. The the output current of the leg is given in (16).

$$i_{sDC} = \frac{P}{v_{dc2}} \tag{16}$$

The resistances R_{arm} and R_s are quite small and can be neglected. Hence, the current in the upper arm can be expressed by (17)

$$i_{uDC} = \frac{P}{v_{dc1}} \tag{17}$$

Finally, i_{lDC} and i_{diffDC} are given in (18) and (19). There are obtained combining (16), (17) and (6).

$$i_{lDC} = \frac{P}{v_{dc2}}(\alpha - 1) \tag{18}$$

$$i_{diffDC} = \frac{P}{2v_{dc2}}(2\alpha - 1) \tag{19}$$

The above equations and (1) define the whole DC system.

C. Quasi-static model of AC components

Secondly, the analysis of AC quasi-static model. Let $\underline{V_{muAC}}$ and $\underline{V_{mlAC}}$ be the complex associated with the AC component of v_{mu} and v_{ml}. They can be expressed in the complex plane as in (20).Let φ be the angle between $-\underline{V_{muAC}}$ and $\underline{V_{mlAC}}$.

$$\begin{cases} \underline{V_{muAC}} = V_{mlAC}e^{j\theta_{vmu}} \\ \underline{V_{mlAC}} = V_{mlAC}e^{j\theta_{vml}} \\ \varphi = \pi + \theta_{vmu} - \theta_{vml} \end{cases} \tag{20}$$

$\underline{V_{diffAC}}$, $\underline{V_{sAC}}$, $\underline{I_{diffAC}}$ and $\underline{I_{sAC}}$ are likely defined. Moreover, the angle between $\underline{V_{diffAC}}$ and $\underline{V_{sAC}}$ and the

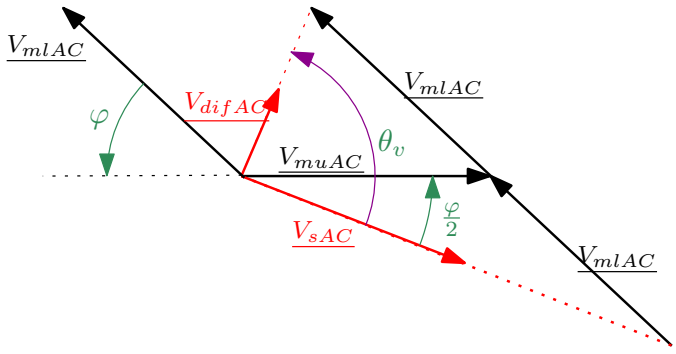

Fig. 3: Fresnel diagram of AC voltages.

angle between $\underline{I_{diffAC}}$ and $\underline{I_{sAC}}$ are respecitbely defined as θ_v and θ.

Based on (6), $\underline{V_{diffAC}}$, $\underline{V_{sAC}}$, $\underline{I_{diffAC}}$ and $\underline{I_{sAC}}$ are expressed by (21) and (22) (once again, the resistance are neglected compared with the inductance).

$$\begin{cases} \underline{V_{diffAC}} = \dfrac{\underline{V_{muAC}} + \underline{V_{mlAC}}}{2} \\ \underline{V_{sAC}} = \dfrac{\underline{V_{muAC}} - \underline{V_{mlAC}}}{2} \end{cases} \tag{21}$$

$$\begin{cases} \underline{i_{diffAC}} = -\dfrac{1}{jL_{arm}\omega}\underline{V_{diffAC}} \\ \underline{i_{sAC}} = -\dfrac{1}{jL_s\omega}\underline{V_{sAC}} \end{cases} \tag{22}$$

Fig. 3 presents the Vector representation of the AC voltages. Firstly, from (22), note that the angle θ and θ_v must be equal. Secondly, the angle φ is a degree of freedom of the control. It impacts the magnitude of the AC components. In order to highlight this relation, the energetic model of the converter is established in the next part.

D. Quasi-static model of the energy stored

Let W_u and W_l be the stored energy in the upper and lower arm. The relations between them and the power is given in (23) and (24).

$$\begin{aligned} \frac{dW_u}{dt} &= \frac{d}{dt}\left(\frac{1}{2}C_{tot}v_{ctotu}^2\right) = v_{mu}i_u \\ &= (v_{diff} + v_s).(i_{diff} + \frac{i_s}{2}) \end{aligned} \tag{23}$$

$$\begin{aligned} \frac{dW_l}{dt} &= \frac{d}{dt}\left(\frac{1}{2}C_{tot}v_{ctotl}^2\right) = v_{ml}i_l \\ &= (v_{diff} - v_s).(i_{diff} - \frac{i_s}{2}) \end{aligned} \tag{24}$$

Once again, the equations are coupled and a change of variable is necessary. W^Σ and W^Δ are the sum and the difference of the upper and lower energy stored. Their behavior is described by (25) and (26).

$$\frac{dW^\Sigma}{dt} = \frac{dW_u}{dt} + \frac{dW_l}{dt} = 2v_{diff}i_{diff} + v_s i_s \tag{25}$$

$$\frac{dW^\Delta}{dt} = \frac{dW_u}{dt} - \frac{dW_l}{dt} = v_{diff}i_s + 2v_s i_{diff} \tag{26}$$

1) Model of the sum of energy W^Σ: Firstly, the sum of energy is analysed by with its average over an AC period. Indeed, controlling the instantaneous energy would adversely affect the current wave generation. The average sum of energy over an AC period (written as $\langle x \rangle_T$) is given in (27). P^Σ corresponds to the required power to manage the sum of energy. During steady state, this power must be null, so the input power is equal to the output power.

$$P^\Sigma = \left\langle \frac{dW^\Sigma}{dt} \right\rangle_T = 2v_{dc1}i_{diffDC} + P\left(\frac{1}{2\alpha} - 1\right) \tag{27}$$

The management of the sum of energy is the same as in the MMC. Thus, it is not detailed in this paper.

2) Model of the difference of energy W^Δ: Secondly, the analysis is carried out for the difference of energies. As showed by [7], the average value of W^Δ can be expressed as in (28).

$$\begin{aligned} P^\Delta &= \left\langle \frac{dW^\Sigma}{dt} \right\rangle_T \\ &= 2P(1-\alpha) - 2L_f\omega I_{sAC}I_{diffAC}sin(\theta) \end{aligned} \tag{28}$$

P^Δ corresponds to the required power to manage the difference of energy. In steady-state, it must be null. So, the relation (29) is extracted.

$$I_{sAC}I_{diffAC}sin(\theta) = \frac{P}{L_f\omega}(1-\alpha) \tag{29}$$

With this last expression, the model of the converter is fully described. With all the equations, it is possible to express all electrical variables as a function of the degree of freedom φ and ω to understand the impact of these on the design and the efficiency.

E. Expression of AC components according to φ and ω

To begin, (29) revealed that the parameters L_f and θ impact the product $I_{sAC}I_{diffAC}$. In order to minimize the latter, the angle θ (and thus θ_v) must be equal to 90°. From fig. 3, this condition fixes the amplitude V_{muAC} and V_{mlAC} as equal (30) since in a right triangle, the

median from the vectors of the right angle is half the hypotenuse.

$$V_{muAC} = V_{mlAC} = V_{mAC} \tag{30}$$

Also from geometrical consideration, V_{sAC} and V_{diffAC} can be deduced as (31) and (32).

$$V_{sAC} = 2V_{mAC}cos\left(\frac{\varphi}{2}\right) \tag{31}$$

$$V_{diffAC} = 2V_{mAC}sin\left(\frac{\varphi}{2}\right) \tag{32}$$

From (31), (32) and (22), the current ratio (33) can be determined.

$$\frac{I_{diffAC}}{I_{sAC}} = \frac{L_s}{L_{arm}}tan\left(\frac{\varphi}{2}\right) \tag{33}$$

To continue, it is now possible to directly link the module of the AC components in the converter with φ and ω. The module of V_{mAC} (34) can be found by combining, (22), (28) and (33),

$$V_{mAC} = \sqrt{\frac{P(1-\alpha)(L_{arm}^2 + 2L_fL_{arm})\omega}{L_f sin(\varphi)}} \tag{34}$$

If $\varphi = \pi/2$, the modulated voltages will be the lowest possible, so a limited number of submodules is required. On the contrary, a smaller value of φ leads to a high voltage and thus more submodules are necessary.

For the currents in the upper and lower arm, there amplitude is given in (35). It is reminded that $\underline{I_{diffAC}}$ and $\underline{I_{sAC}}$ are orthogonal. Therefore, $\underline{I_{uAC}}$ and $\underline{I_{lAC}}$ have the same module I_{AC} given in (36).

$$\begin{aligned} I_{uAC} &= \left|\underline{I_{diffAC}} + \frac{\underline{I_s}}{2}\right| \\ I_{lAC} &= \left|\underline{I_{diffAC}} - \frac{\underline{I_s}}{2}\right| \end{aligned} \tag{35}$$

$$I_{AC} = \sqrt{(I_{diffAC})^2 + \left(\frac{I_{sAC}}{2}\right)^2} \tag{36}$$

Injecting (22), (32), (31) and (34), I_{AC} can be expressed as in (37)

$$I_{AC} = A\frac{cos\left(\frac{\varphi}{2}\right)}{sin(\varphi)} * \sqrt{\left(\frac{L_s}{L_{arm}}tan\left(\frac{\varphi}{2}\right)\right)^2 + \frac{1}{4}} \tag{37}$$

$$\text{with } A = \frac{2}{L_s}\sqrt{\frac{P(1-\alpha)(L_{arm}^2 + 2L_fL_{arm})\omega}{L_f}}$$

A direct interpretation of this formula is not straight forward. However, it allows a analytical study of the impact of the degree of freedom φ and ω on the electrical variables.

IV. Interaction between frequency and angle on M2DC design and efficiency

The analysis is carried out for a three-phase (fig 1) converter of 600 MW whose parameters are displayed in table I. As the fault behavior is out of the scope, the submodules used are half-bridge in order to minimize the losses. In this case, V_{mACmac} admissible is defined by (38) because the generation of negative voltage is not possible. This limits the values of φ as showed by (34).

$$V_{mACmac} = \frac{1}{\sqrt{2}}\min(v_{dc2}; v_{dc1} - v_{dc2}) \tag{38}$$

Parameter	Value
v_{dc1}	320 kV
v_{dc2}	250 kV
R_{arm}	4 mΩ
L_{arm}	4 mH
R_f	50 mΩ
L_f	120 mH

TABLE I: Parameters of the M2DC converter

As for the frequency, it must respect the constraints of technical feasibility. This is why, the range of variation is limited between 50Hz and 350Hz.

A. Impact of φ and ω on electrical components

The maximum values of modulated voltage and the arms currents according to φ and ω are represented in fig. 4 and fig. 5. In 4, the function displayed corresponds to both upper and lower arm. Only the scale changes between the two as represented by the two z-axes, $V_{mu_{max}}/V_{uDC}$ on the left and $V_{ml_{max}}/V_{lDC}$

Fig. 4 and (34) indicates that a higher frequency leads to higher modulated voltage. As for the angle, the higher it is, the smaller the voltage.

For the currents, fig. 5a and fig. 5b present there evolution. A higher frequency results in lower currents while a higher angle increase them. In these figures, some values are not feasible with current interrupter like IGBT, which would lead to an increased number of arms.

This analysis alone cannot define the optimal operating point of the converter. To do so, the design of the capacitors and the efficiency of the converter must be considered.

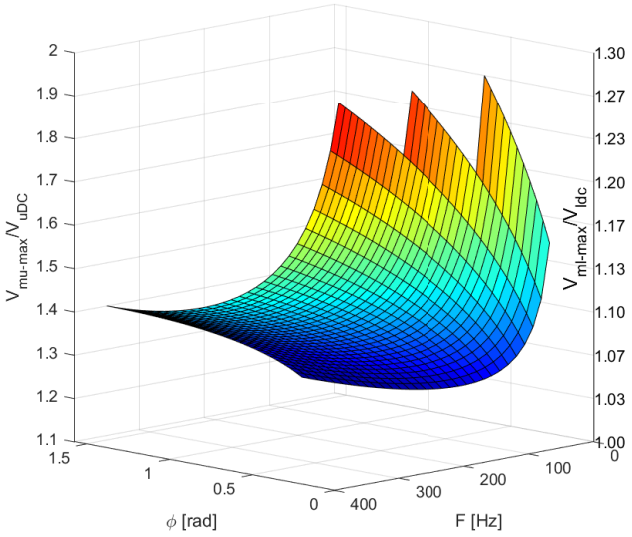

Fig. 4: Maximum modulated voltage as a function of φ and ω.

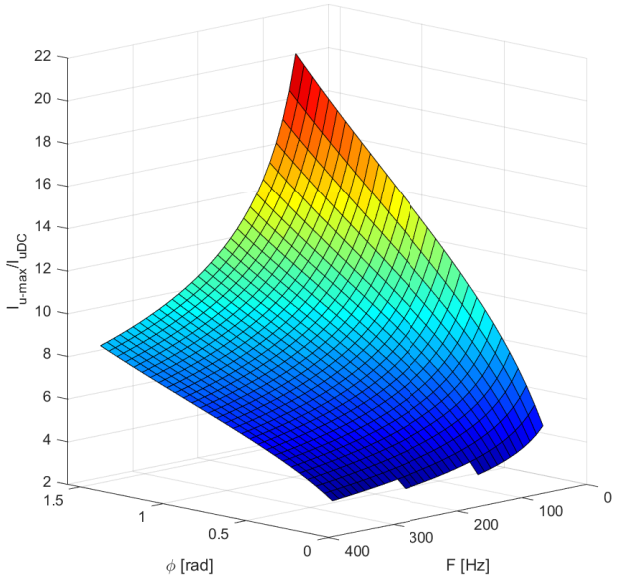

(a) Maximum upper arm current.

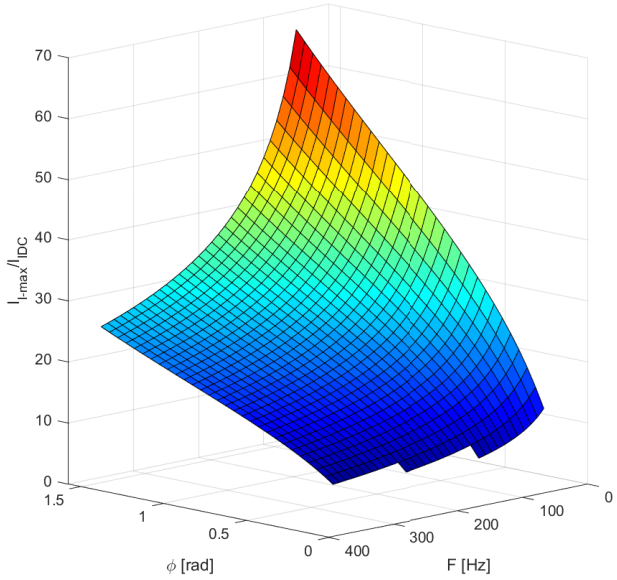

(b) Maximum lower arm current.

Fig. 5: Maximum arm currents as a function of φ and ω.

B. *Impact of φ and ω on the capacitor design*

The capacitor value of one arm is determined in order to limit the ripple of voltage to $\pm 10\%$. To calculate it, the fluctuating power is first determined thanks to equations (3), (34) and (37). Then, it is possible to estimate the fluctuation of energy in one arm. Knowing this fluctuation, the capacitor value is determined to limit the voltage ripple thanks to (39).

$$\frac{1}{2} C_{tot} \Delta V_{tot}^2 = \Delta E \tag{39}$$

It is usual to represents the energy stored in the capacitors compared with the nominal power as presented in (40). In the M2DC, the nominal voltage of a capacitor arm is V_{ctoti} and the power is $\frac{P_{nom}}{3}$.

$$H_c = \frac{\frac{1}{2} C V^2}{P} \tag{40}$$

The results for H_c are exposed in fig. 6. The capacitor needed is bigger when the frequency decreases and the angle φ increases. More precisely, the relation between C_{tot} and H_c can be approximated by a line whose slope is inversely proportional to the frequency. The lower arm needs more energy stored because the fluctuating power is higher. Indeed, although the AC components are the same, the DC current is higher, thus so is the instantaneous power.

From the equivalent arm capacitor value, the one of the submodules is obtained by multiplying by the number of these. Note that the number of submodules is determined by the maximum modulated voltage divided by the design sub-module voltage (usually 1600V). This result is the same as fig. 6. Capacitor values are between $1.35mF$ and $207mF$ for the upper arm and $11.5mF$ and $230mF$ for the lower arm.

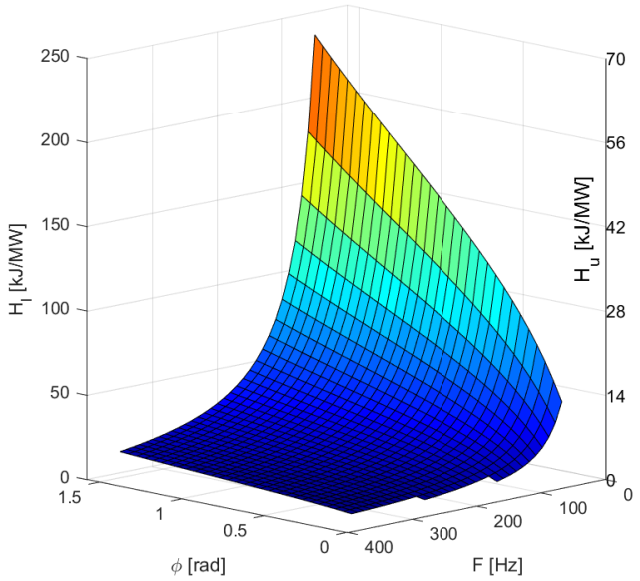

Fig. 6: Stored energy needed in one arm as a function of φ and ω.

In conclusion, as for the capacitor design, the frequency should be chosen high and the angle small. However, a high frequency increases the commutation losses. An analysis of the efficiency is thus required.

C. Impact of φ and ω on the losses

To estimate the losses, a numerical approach is adopted with MATLAB-Simulink, one leg is simulated with its voltage balancing algorithm [10]. From this simulation, submodule voltages, arm currents and state of the interrupter are retrieved. It is then possible to calculate the losses in the arms [8]. The submodule chosen for this study is the IGBT 5SJA 3000L520300 from ABB [11].

Fig. 7a and fig. 7b display the conduction losses and commutation losses respectively for upper arm and lower arm. As predicted, commutation losses increase with the frequency. As for conduction losses, they are inversely proportional to the frequency. Note that the upper arms generate less losses than the lower arm despite its higher current (equal in AC but higher in DC). Indeed, it is composed of less submodules because its rated voltage is lower than the other arm. In fact, in this converter the upper arms need 88 submodules whereas the lower arms need 200.

Fig. 8 shows the total losses in the converter. The optimal operating point is with the minimum angle possible and a frequency near $70Hz$. Then, the losses

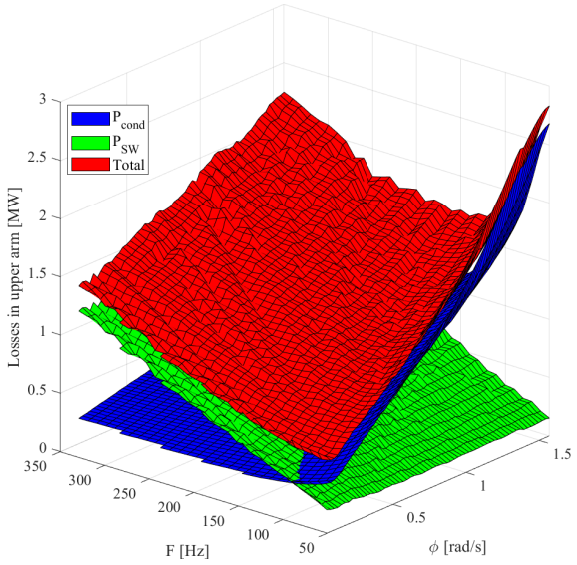

(a) Estimated losses in upper arm.

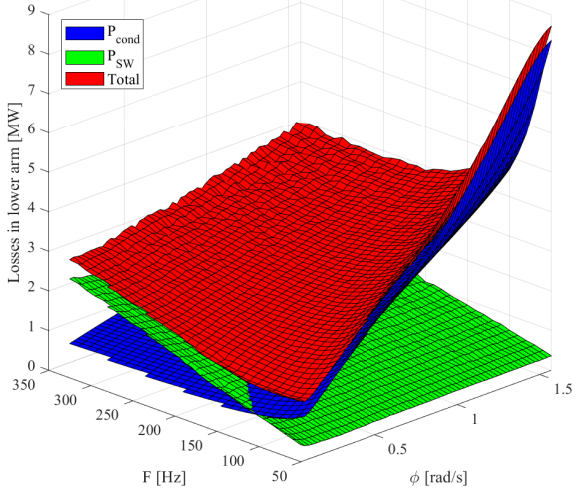

(b) Estimated losses in lower arm.

Fig. 7: Estimated losses in the converter arms as a function of φ and ω.

are up to $6.11MW$ for the nominal power $600MW$. So, the overall efficiency is 98.97%. However, this choice requires substantial capacitors as shown by table II. If the frequency is increased, the capacitors take lower values but it will generate additional losses. the converter cost and footprint (CAPEX) will be reduced but the operation cost (OPEX) will be higher.

V. Conclusions

This paper presents a full quasi-static study of the modular multilevel DC converter (M2DC) which is an

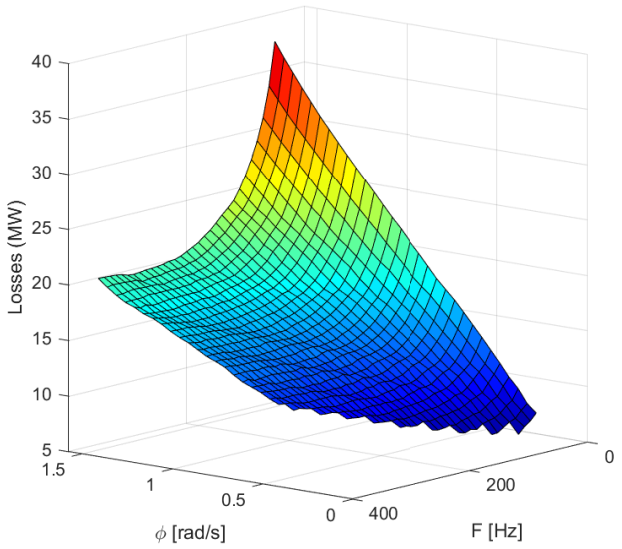

Fig. 8: Total losses in the converter as a function of φ and ω.

f (Hz)	φ (rad)	C_{SMu} (mF)	C_{SMl} (mF)	Losses (MW)	η (%)
70	0.096	22.2	31.6	6.11	98.97
120	0.096	8.00	12.5	6.35	98.94
150	0.120	5.40	9.50	6.86	98.85
200	0.120	3.00	6.00	7.90	98.68

TABLE II: Design and efficiency of the M2DC according to the choice of φ and ω.

attractive non-isolated topology for HVDC networks. First, the degree of freedom in the control are highlighted : the frequency and the angle. Then, the impact of these on the design and efficiency is studied. It is concluded that the minimal feasible angle should be chosen. As for the frequency, it should between 60 and 150Hz depending on the footprint and cost desired.

In this paper, the converter had three phases like the AC-DC MMC. It seems like a good compromise between losses and number of components. An investigation on the optimal number of phase should be realized as future works. Moreover, the performance of the M2DC should be compared with other DC-DC converter such as the MMC-Autotransformer or the MMC-DAB.

REFERENCES

[1] G. P. Adam, I. A. Gowaid, S. J. Finney, D. Holliday, and B. W. Williams, "Review of dc–dc converters for multi-terminal HVDC transmission networks," *IET Power Electronics*, vol. 9, no. 2, pp. 281–296, Feb. 2016. [Online]. Available: https://onlinelibrary.wiley.com/doi/10.1049/iet-pel.2015.0530

[2] J. D. Páez, D. Frey, J. Maneiro, S. Bacha, and P. Dworakowski, "Overview of DC–DC Converters Dedicated to HVdc Grids," *IEEE Transactions on Power Delivery*, vol. 34, no. 1, pp. 119–128, Feb. 2019, conference Name: IEEE Transactions on Power Delivery.

[3] J. A. Ferreira, "The Multilevel Modular DC Converter," *IEEE Transactions on Power Electronics*, vol. 28, no. 10, pp. 4460–4465, Oct. 2013, conference Name: IEEE Transactions on Power Electronics.

[4] J. Peralta, H. Saad, S. Dennetiere, J. Mahseredjian, and S. Nguefeu, "Detailed and averaged models for a 401-level MMC-HVDC system," in *2013 IEEE Power & Energy Society General Meeting*, Jul. 2013, pp. 1–1, iSSN: 1932-5517.

[5] Y. Li, F. Gruson, P. Delarue, and P. Le Moigne, "Design and control of modular multilevel DC converter (M2DC)," in *2017 19th European Conference on Power Electronics and Applications (EPE'17 ECCE Europe)*, Sep. 2017, pp. P.1–P.10.

[6] H. Yang and M. Saeedifard, "A Capacitor Voltage Balancing Strategy With Minimized AC Circulating Current for the DC–DC Modular Multilevel Converter," *IEEE Transactions on Industrial Electronics*, vol. 64, no. 2, pp. 956–965, Feb. 2017, conference Name: IEEE Transactions on Industrial Electronics.

[7] F. Gruson, Y. Li, P. L. Moigne, P. Delarue, F. Colas, and X. Guillaud, "Full State Regulation of the Modular Multilevel DC Converter (M2DC) Achieving Minimization of Circulating Currents," *IEEE Transactions on Power Delivery*, vol. 35, no. 1, pp. 301–309, Feb. 2020, conference Name: IEEE Transactions on Power Delivery.

[8] J. Freytes, F. Gruson, P. Delarue, F. Colas, and X. Guillaud, "Losses estimation method by simulation for the modular multilevel converter," in *2015 IEEE Electrical Power and Energy Conference (EPEC)*, Oct. 2015, pp. 332–338.

[9] P. Delarue, F. Gruson, and X. Guillaud, "Energetic macroscopic representation and inversion based control of a modular multilevel converter," in *2013 15th European Conference on Power Electronics and Applications (EPE)*, Sep. 2013, pp. 1–10.

[10] P. M. Meshram and V. B. Borghate, "A Simplified Nearest Level Control (NLC) Voltage Balancing Method for Modular Multilevel Converter (MMC)," *IEEE Transactions on Power Electronics*, vol. 30, no. 1, pp. 450–462, Jan. 2015, conference Name: IEEE Transactions on Power Electronics.

[11] 5SJA 3000L520300, "ABB Stakpak modules," Product specification sheet, Mar. 2020. [Online]. Available: https://new.abb.com/semiconductors/stakpak